NeuroImage: Clinical 35 (2022) 103080

Contents lists available at ScienceDirect

NeuroImage: Clinical

journal homepage: www.elsevier.com/locate/ynicl

Metabolic brain pattern in dementia with Lewy bodies: Relationship to Alzheimer's disease topography

Matej Perovnik [a,b,*], Petra Tomše [c], Jan Jamšek [c], Chris Tang [d], David Eidelberg [d], Maja Trošt [a,b,c]

[a] Department of Neurology, University Medical Center Ljubljana, Zaloška cesta 2, 1000 Ljubljana, Slovenia
[b] Faculty of Medicine, University of Ljubljana, Vrazov trg 2, 1000 Ljubljana, Slovenia
[c] Department of Nuclear Medicine, University Medical Center Ljubljana, Zaloška cesta 2, 1000 Ljubljana, Slovenia
[d] Center for Neurosciences, The Feinstein Institutes for Medical Research, 350 Community Drive, Manhasset, NY 11030, USA

ARTICLE INFO

Keywords:
Dementia with Lewy bodies
Alzheimer's disease
Biomarker
Metabolic brain imaging
FDG PET
Network analysis
Scaled subprofile model/principal component analysis (SSM/PCA)

ABSTRACT

Purpose: Dementia with Lewy bodies (DLB) is the second most common neurodegenerative dementia, that shares clinical and metabolic similarities with both Alzheimer's and Parkinson's disease. In this study we aimed to identify a DLB-related pattern (DLBRP), study its relationship with other metabolic brain patterns and explore its diagnostic and prognostic value.

Methods: A cohort of 79 participants with DLB, 63 with dementia due to Alzheimer's disease (AD) and 41 normal controls (NCs) and their 2-[^{18}F]FDG PET scans were analysed for identification and validation of DLBRP. Voxel-wise correlation and multiple linear regression were used to study the relation between DLBRP and Alzheimer's disease-related pattern (ADRP), Parkinson's disease-related pattern (PDRP) and PD-related cognitive pattern (PDCP). Diagnostic and prognostic value of DLBRP and of modified DLBRP after accounting for ADRP overlap (DLBRP $\perp$ ADRP), were explored.

Results: The newly identified DLBRP shared topographic similarities with ADRP (R^2 = 24%) and PDRP (R^2 = 37%), but not with PDCP. We could accurately discriminate between DLB and NC (AUC = 0.99) based on DLBRP expression, and between DLB and AD (AUC = 0.87) based on DLBRP $\perp$ ADRP expression. DLBRP expression correlated with cognitive impairment, but the correlation was lost after accounting for ADRP overlap. DLBRP and DLBRP $\perp$ ADRP correlated with patients' survival time.

Conclusion: DLBRP has proven to be a specific metabolic brain biomarker of DLB, sharing similarities with ADRP and PDRP, but not PDCP. We observed a similar metabolic mechanism underlying cognitive impairment in DLB and AD. DLB-specific metabolic changes were more detrimental for overall survival.

1. Background

Dementia with Lewy bodies (DLB) is an α-synucleinopathy and the second most common neurodegenerative dementia. It is characterized by dementia and one or more core features of the disease: parkinsonism, visual hallucinations, fluctuating cognition or rapid eye movement sleep behaviour disorder (RBD) (Arnaoutoglou et al., 2019). Unfortunately, DLB continues to be both under-diagnosed (Vann Jones and O'Brien, 2014) and misdiagnosed; up to 20% of the clinically-made DLB diagnoses are erroneous (Rizzo et al., 2018). An accurate diagnosis is important in determining the prognosis of the disease, which is worse in DLB compared to the prognosis of the most common dementia that is caused by Alzheimer's disease (AD) (Mueller et al., 2017). DLB and Parkinson's disease dementia (PDD) also share many clinical and pathological features, thus making the diagnosis between the two diseases hinge on the arbitrarily set "1-year rule": dementia that occurs within one-year of parkinsonism is termed DLB (McKeith et al., 2017). Research and debate on the similarities and differences between these two diseases is still ongoing (Jellinger, 2018).

DLB biomarkers are needed to improve diagnostic accuracy, to provide prognostic information, and to study potential novel therapies (Oppedal et al., 2019). Since specific biomarkers of α-synuclein are still under development (Hansson, 2021), we can turn to metabolic brain imaging with 2-[^{18}F]fluoro-2-deoxy-D-glucose positron emission tomography (2-[^{18}F]FDG PET), which is a widely accessible, relatively affordable, and a non-invasive imaging technique that is already

* Corresponding author at: Department of Neurology, University Medical Center Ljubljana, Zaloška cesta 2, 1000 Ljubljana, Slovenia.
E-mail address: matej.perovnik@kclj.si (M. Perovnik).

https://doi.org/10.1016/j.nicl.2022.103080
Received 21 March 2022; Received in revised form 26 May 2022; Accepted 5 June 2022
Available online 8 June 2022

considered a supportive biomarker of DLB (McKeith et al., 2017). Metabolic changes in DLB are characterized by hypometabolism in the occipital, parietal and temporal lobes (Brown et al., 2014), and relatively spared posterior cingulate metabolism with hypometabolism of the precuneus, i.e. cingulate island sign (Raffa et al., 2020). However, regional metabolic changes in DLB can overlap with those observed in AD (Meles et al., 2017). Clinically, the most frequent misdiagnosis of DLB is AD (Shim et al., 2013). Therefore, a search for metabolic brain biomarkers that would be able to differentiate between the two diseases is warranted. Multivariate analysis approaches, such as scaled subprofile model/principal component analysis (SSM/PCA), applied to 2-[^{18}F]FDG PET images can reveal characteristic metabolic brain patterns. The expression of these metabolic brain patterns can be prospectively quantified and correlated with subjects' clinical measures (Spetsieris and Eidelberg, 2011). An approach similar to the SSM/PCA model already identified core feature-specific patterns in DLB, which exhibit stable hypermetabolic regions in the medial temporal lobe, orbitofrontal cortex, cerebellum, pons, basal ganglia, thalami and sensorimotor cortex across features, but different hypometabolic regional involvement related to each core feature (Morbelli et al., 2019). Patterns of the two clinically overlapping syndromes, namely AD-related pattern (ADRP) (Perovnik et al., 2020) and PD-related pattern (PDRP) (which is related to severity of motor symptoms (Schindlbeck and Eidelberg, 2018)), as well as PD-related cognitive pattern (PDCP) (which is related to cognitive impairment (Trošt et al., 2019)) have been identified and validated previously. However, their relation to DLB metabolic changes remains to be explored. Furthermore, DLB also pathologically overlaps with AD, with >50% of DLB patients exhibiting Alzheimer's pathology, (i. e. amyloid β deposits, on *post-mortem* examination (Hepp et al., 2016)) and nearly 40% have positive Alzheimer's CSF biomarkers *in vivo* (Lemstra et al., 2017). This renders amyloid β biomarkers less accurate in differential diagnosis between the two disorders (Watson and Colloby, 2016). The effect of concomitant Alzheimer's pathology on clinical and imaging features in DLB has been shown before (Lee et al., 2018), but remains to be fully elucidated (Watson and Colloby, 2016).

The aims of this study were to (i) identify and validate a unified DLB-related pattern (DLBRP) in a new population, (ii) examine its spatial relation to metabolic patterns of AD and PD, (iii) study the effect of concomitant Alzheimer's pathology on pattern expression, and (iv) explore diagnostic and prognostic clinical value of the expression of newly identified DLBRP.

2. Methods

2.1. Participants

We analysed 79 patients with probable DLB, 63 patients with AD and 41 normal controls (NCs) who all underwent 2-[^{18}F]FDG PET brain imaging between January 2010 and April 2019 at the University Medical Center Ljubljana (UMCL), Slovenia. Patients with DLB were diagnosed according to the latest clinical criteria (McKeith et al., 2017). To improve clinical diagnostic confidence, we included only DLB patients with diagnosis confirmed at a follow-up visit at least 12 months after being first diagnosed ($n = 70/79$) or at least one year ($M = 3$ years) after symptoms onset when first diagnosed ($n = 9/79$). 76 cases had two or more core features of the disease and three cases had just one core feature but also one indicative biomarker, namely imaging of the presynaptic dopaminergic transporter (DaTSCAN™) to make a probable DLB diagnosis. Mini mental state examination (MMSE) (Rakusa et al., 2006) score within one year of imaging ($Mdn = 24$ days) was obtained. For the deceased individuals we calculated the time from imaging to death. NCs completed clinical neurological and neuropsychological examination and 2-[^{18}F]FDG PET brain imaging for purposes of an earlier research project (Tomše et al., 2017). In AD patients, the diagnosis was confirmed by CSF biomarkers profile (Jack et al., 2018).

2.2. Cerebrospinal fluid analysis

Thirty-two patients with DLB and all AD patients underwent lumbar puncture (LP) and CSF analysis within 18 months of 2-[^{18}F]FDG PET scanning, with a mean of 6 months in DLB and 9 months in AD. CSF samples were centrifuged, aliquoted and stored at −80 °C until biomarker analysis was performed at the Department of Neurology, UMCL. CSF $A\beta_{42}$, phosphorylated tau (p-tau) and total tau protein (t-tau) were measured routinely, whereas $A\beta_{40}$ was determined additionally in 22 CSF (20 AD and 2 DLB) samples with ambiguous $A\beta_{42}$ result (650–815 pg/ml). Biomarker analyses were performed according to manufacturers' instructions using Innotest (Fujirebio, Europe) immunoassays with intra-assay variability < 5%. Between-assay coefficients of variation for $A\beta_{42}$, $A\beta_{40}$, p-tau and t-tau were 5.8%, 8.3%, 4.4% and 8.2%, respectively, as determined by the longitudinal quality control sample. Locally validated biomarker cut-off levels were used to define Alzheimer's CSF profile as: $A\beta_{42} < 650$ pg/ml or $A\beta_{42}/A\beta_{40} < 0.0077$ (A +), p-tau > 60 pg/ml (T +) and t-tau > 400 pg/ml (N +). A+/T+/N± was considered as Alzheimer's disease and A+/T−/N± as Alzheimer's pathologic change (Jack et al., 2018).

2.3. Image acquisition

2-[^{18}F]FDG PET images were acquired at the Department of Nuclear Medicine, UMCL with Siemens Biograph mCT PET/CT (Siemens Healthineers, Erlangen, Germany) according to European Association of Nuclear Medicine (EANM) guidelines (Varrone et al., 2009) as described previously (Tomše et al., 2017).

DaTSCAN™ was performed at the Department of Nuclear Medicine, UMCL, using a Siemens Symbia Intevo SPECT/CT system (Siemens Healthineers, Munich, Germany) using [^{123}I]I-ioflupane ([^{123}I]I-FP-CIT), following EANM recommendations (Darcourt et al., 2010). To minimize thyroid exposure to radiation, all patients received 90 mg of iodide (KI *p.o.*) 1 h prior to i.v. administration of 185 MBq of [^{123}I]I-FP-CIT. SPECT images were acquired 4 h after the radiotracer application, using a LEHR collimator, with a photopeak of 159 KeV ± 15%, using a circular orbit in step-and-shoot mode (60 steps of 25 s) over 360°, with a 128 × 128 matrix, using a zoom of 1.78. Images were reconstructed using the Flash-3D iterative algorithm (2 iterations, 15 subsets), using scatter correction, a 3D Gaussian filter (FWHM = 6 mm) and AC correction using the Chang algorithm ($\mu = 0{,}12$ cm^{-1}).

2.4. Image pre-processing

2-[^{18}F]FDG PET scans were pre-processed with SPM12 (Wellcome Trust Centre for Neuroimaging, Institute of Neurology, London, UK) running on Matlab R2019a (Mathworks Inc., Natick, MA) using an in-house pipeline. Briefly, we performed 3D affine transformation, followed by brain extraction by segmenting the skull based on the tissue probability map and spatial normalization onto a PET template in Montreal Neurological Institute brain space using old normalization function. Finally, the images were smoothed with an isotropic 3D Gaussian kernel of 10 mm FWHM.

2.5. Image analysis

2.5.1. Identification and validation of DLB-related pattern

For the identification of the DLBRP we applied SSM/PCA (ScAnVP, Center for Neuroscience, Feinstein Institutes for Medical Research, NY, USA) to 2-[^{18}F]FDG PET scans of 20 randomly selected DLB patients and 20 age- and sex-matched NC. The SSM/PCA procedure was described in detail before (Meles et al., 2021; Spetsieris and Eidelberg, 2011). The output of the procedure are principal components (PCs) and the corresponding subject scores, which underwent further analysis to identify DLBRP. This analysis was limited to all PCs that explained at least 5% of the total variance. Subject scores for these PCs were entered into a series

of logistic regression models, with the group as the dependent variable and the subject scores for the PCs as the independent variables in each model. The model with the lowest Akaike Information Criterion (AIC) score was selected. For the validation of the newly identified DLBRP we used topographic profile rating (TPR) (Spetsieris and Eidelberg, 2011) and 2-[^{18}F]FDG PET scans from 59 DLB, 63 AD and 21 NC not included in the identification cohort (Table 1). The raw scores were Z-transformed based on the mean pattern expression and standard deviation of subjects scores in the NC identification cohort (NC1).

2.5.2. Relation to other metabolic patterns

We assessed the topographic relationship between newly identified DLBRP and previously identified ADRP (Perovnik et al., 2020) as well as two metabolic patterns observed in PD: PDRP (Tomše et al., 2017) and PDCP (Huang et al., 2007) on a voxel-by-voxel basis using Pearson's correlation corrected for spatial autocorrelation (Ko et al., 2014). Furthermore, we used multiple linear regression to calculate total variance explained and relative importance of ADRP, PDRP and PDCP voxel weights on DLBRP voxel weights with the CAR method (Zuber and Strimmer, 2011), which adjusts for correlation among explanatory variables, implemented in the *relaimpo* R package (Grömping, 2006). Finally, we examined topographic overlap between patterns by identifying voxels with weights above 1 or below −1 in each of the three pattern pairs. DLBRP-specific regions were then determined as voxels with weights above 1 or below −1 in DLBRP but not in the other metabolic pattern. Overlapping and DLB-specific regions were localized with MRIcroGL (version 1.2.20200331, (Rorden and Brett, 2000)).

2.5.3. Identification of DLB-related pattern without AD-network component

First, we calculated ADRP expression in DLB patients using the TPR algorithm. The scores were Z-transformed based on the mean pattern expression and standard deviation of subjects scores in the NC group used for pattern identification (Perovnik et al., 2020). Then, to eliminate any possible contribution of ADRP on the DLBRP, we performed SSM/PCA of orthogonal components using *vp_ssm_voxOpca* function implemented in ScAnVP. This special application of SSM is used to remove PCs that might influence the analysis, i.e. ADRP in our case, by removing them from the 2-[^{18}F]FDG PET scans used for the DLBRP identification. Then, SSM/PCA was performed in the reduced, orthogonal space (Spetsieris and Eidelberg, 2011). The pattern identified in this orthogonal space was termed DLBRP ⊥ ADRP, and again the new pattern's expression was evaluated prospectively in patients not used for pattern identification using TPR algorithm (Table 1).

2.6. Effect of Alzheimer's pathology on patterns expression

To examine the effect of Alzheimer's pathology on the expression of the patterns, we divided DLB patients based on their CSF results into two groups, i. e. with and without concomitant Alzheimer's pathology. Patients on CSF Alzheimer's continuum (either A+/T+ or A+/T−) were considered as having concomitant Alzheimer's pathology. We compared the two DLB subgroups by using a two-sample *t*-test according to the general linear model at each voxel using SPM12. To evaluate results, we set the peak threshold at $p < 0.01$ (uncorrected) and visualized the results with xjView toolbox (https://www.alivelearn.net/xjview). Significant regions were localized with BioImage Suite (https://bioimagesuiteweb.github.io/webapp/mni2tal.html). Additionally, we calculated the expressions of DLBRP, ADRP and DLBRP ⊥ ADRP in both DLB subgroups.

2.7. Statistical analysis

Student's independent-sample *t*-test or one-way analysis of variance (ANOVA) with post hoc Tukey HSD was used to examine differences in age, MMSE and disease duration in the NC and patient groups. When comparing small groups with unequal variances we used Welch's *t*-test (Delacre et al., 2017). Fisher's exact test for count data was used to examine differences in sex distribution. One-way ANCOVA with post hoc Tukey HSD was used to assess group differences in pattern expressions while controlling for differences in age, sex and MMSE across groups. We used *pROC* R package (Robin et al., 2011) to calculate the area under the curve (AUC); specificity, sensitivity, positive and negative predictive values were determined by Youden's index. Pearson's correlation coefficient was used for correlational analyses. All statistical analyses were conducted in RStudio version 1.3.1093, R version 3.6.0 (R Core Team, 2019) and figures were produced with *ggplot2* R package (Wickham, 2016). Results were considered significant at $p < 0.05$ (two-tailed).

3. Results

Subjects demographic and clinical data are presented in Table 1.

3.1. DLBRp

3.1.1. Identification

For the DLBRP identification, DLB1 and NC1 cohorts were analysed. They did not differ in mean age ($t(38) = 1.32$, $p = 0.19$) or sex

Table 1
Demographic data for identification and validation cohorts.

	Identification		Validation			p value	
						Ident	Val
	NC1	DLB1	NC2	DLB2	AD		
N	20	20	21	59	63		
Age (y)	68.8 ± 5.4	71.5 ± 7.1	61.9 ± 6.8	76.4 ± 5.8	72.9 ± 8.8	0.19	< 0.001†
Sex (f/m)	9/11	6/14	19/2	22/37	31/32	0.51	< 0.001††
Disease duration (y)	/	3.9 ± 2.1 (n = 19)	/	3.9 ± 2.1 (n = 55)	3.6 ± 2.3 (n = 54)		0.39
MMSE	28.8 ± 1.1 (n = 16)	20.1 ± 5.2 (n = 15)	29.2 ± 0.9 (n = 16)	21.5 ± 5.0 (n = 39)	18.0 ± 5.1 (n = 59)	< 0.001	< 0.001†††
Parkinsonism	/	20/20	/	59/59	/	–	
Visual hallucinations	/	15/20	/	43/59	/		1.00
Fluctuating cognition	/	10/20	/	24/59	/		0.60
REM sleep behavior disorder	/	9/20	/	26/59	/		1.00
Repeated falls	/	3/20	/	12/59	/		0.75
Autonomic dysfunction	/	10/20	/	26/59	/		0.80
DaTSCAN™ (abnormal/total)	/	11/11	/	14/17	/		0.26

All the data is presented as mean ± SD. NC – normal control, DLB – dementia with Lewy bodies, AD – dementia due to Alzheimer's disease, MMSE – Mini Mental State Examination. †DLB2 > AD > NC2, ††NC2 different from DLB2 and AD, †††NC2 > DLB2 > AD.

distribution ($p = 0.51$). The DLB1 had lower MMSE scores than NC1, $t(29) = -6.46$, $p < 0.0001$ (Table 1).

DLBRP was defined as the first PC (34.9% variance accounted for (VAF)) and was characterized by relatively reduced bilateral metabolic activity in the occipital, inferior parietal and inferior temporal cortices and precuneus, which co-varied with relatively increased metabolic activity in bilateral pallidum, putamen, amygdala, hippocampi, parahippocampi, cerebellar vermis and cortex and pons (Fig. 1). The pattern's expression was significantly higher in DLB1 ($M = 6.0$, $SD = 1.5$) compared to NC1 ($M = 0.0$, $SD = 1.0$), $t(38) = 14.78$, $p < 0.0001$ (Fig. 2). DLBRP expression did not correlate with age ($r(18) = -0.14$, $p = 0.56$), nor with MMSE ($r(13) = -0.39$, $p = 0.15$) in DLB1.

3.1.2. Validation

There was a significant difference in age between the validation groups ($F(2, 140) = 29.9$, $p < 0.001$). Post hoc comparisons indicated that DLB2 and AD were each older than NC2 ($p < 0.001$) and that DLB2 was older than AD ($p = 0.02$). Sex distributions differed for NC2 and DLB2 ($p < 0.001$) and NC2 and AD ($p < 0.001$), but not for DLB2 and AD ($p = 0.20$). There was a significant difference in MMSE scores between the validation groups ($F(2, 111) = 36.4$, $p < 0.001$). Post hoc comparisons indicated that the MMSE scores were significantly higher in NC2 compared to DLB2 and AD, both $p < 0.001$. DLB2 had higher MMSE scores than AD ($p = 0.001$). Disease duration did not differ between DLB2 and AD, $t(107) = 0.86$, $p = 0.39$ (Table 1).

DLBRP expression differed in the validation groups ($F(2, 108) = 27.0$, $p < 0.001$) even after controlling for age, sex and MMSE differences. Post hoc comparisons showed that covariate adjusted mean DLBRP expression was significantly higher in DLB2 than in NC2 (difference = 3.3, $t = 5.49$, $p < 0.001$) and AD (difference = 2.08, $t = 6.06$, $p < 0.001$), but not between AD and NC2 (difference = 1.26, $t = 2.02$, $p = 0.11$) (Fig. 2). DLBRP expression did not correlate with age ($r(57) = -0.12$, $p = 0.38$), but did so with MMSE ($r(37) = -0.35$, $p = 0.03$) in DLB2.

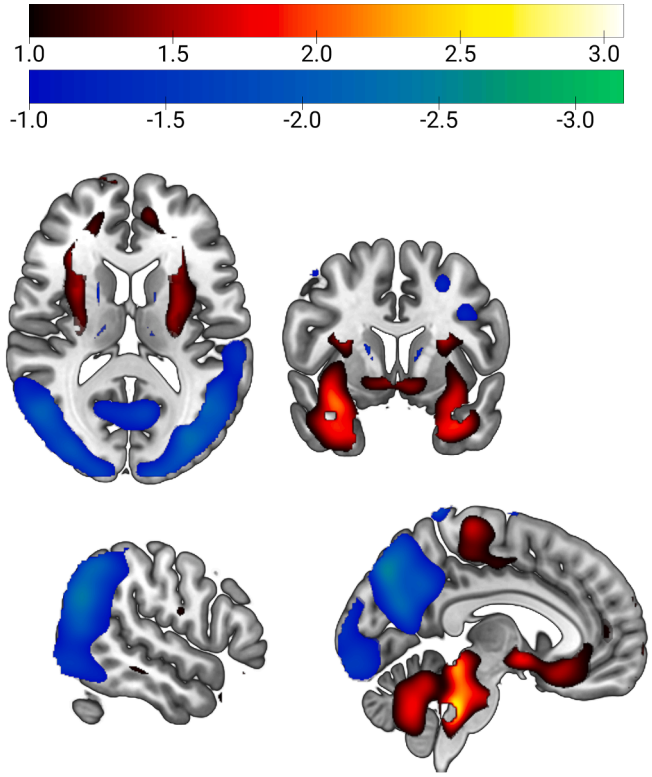

Fig. 1. Dementia with Lewy bodies-related pattern (DLBRP). DLBRP was characterized by relatively reduced bilateral metabolic activity (color-coded blue to green) in occipital, inferior parietal and inferior temporal cortices and precuneus which co-varied with relatively increased metabolic activity (color-coded red to white) in bilateral pallidum, putamen, amygdala, hippocampi, parahippocampi, cerebellar vermis and cortex and pons. (For interpretation of the references to color in this figure legend, the reader is referred to the web version of this article.)

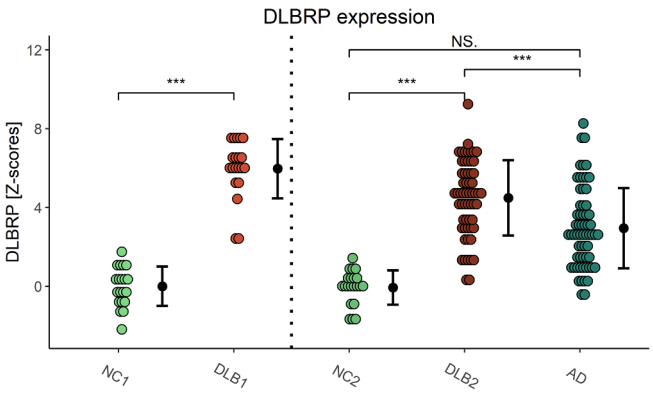

Fig. 2. Dementia with Lewy bodies-related pattern (DLBRP) expression in identification (NC1 and DLB1) and validation (NC2, DLB2 and AD) groups. Data are Z-transformed based on the pattern expression in NC1 group. Means (SD) are presented to the right of individual data. NC – normal controls, DLB – dementia with Lewy bodies, AD – dementia due to Alzheimer's disease. ***p < 0.001, NS. – non-significant difference after adjusting for age, sex and MMSE.

Adjusted mean DLBRP expression did not differ between NC1 and NC2 after controlling for age, sex and MMSE (difference = 0.15, $t = 0.34$, $p = 0.74$). Adjusted mean DLBRP expression differed between DLB1 and DLB2 even after controlling for age, sex and MMSE (difference = 1.21, $t = 2.31$, $p = 0.025$).

3.2. Relationship between DLBRP and other metabolic brain patterns

We observed a close correlation between DLBRP and ADRP ($r = 0.692$, $p < 0.001$; corrected for spatial autocorrelation) as well as between DLBRP and PDRP ($r = 0.775$, $p < 0.001$; corrected for spatial autocorrelation) (Fig. 3). Correlation between DLBRP and PDCP was non-significant ($r = 0.348$, $p = 0.05$; corrected for spatial autocorrelation).

Multiple linear regression showed that 64.4% of the variance in voxel weights of DLBRP was predicted from the three other patterns, leaving 35.6% variance unexplained. A decomposition of R^2 among explanatory variables showed that 37.4% is accounted by PDRP, 24.4% by ADRP and 2.6% by PDCP.

The overlap between DLBRP and ADRP was seen in the hypometabolic regions of the parietal cortices, angular gyri, occipital superior and middle cortices, precuneus and cuneus; hypermetabolic regions were seen in the insula, amygdala, cerebellar vermis and cortex and pons (Fig. 3a). DLBRP was additionally comprised of hypometabolic regions in the occipital and inferior temporal cortices; hypermetabolic regions were seen in the bilateral putamen, pallidum, hippocampi and parahippocampi.

The overlap between DLBRP and PDRP was seen in hypometabolic regions in precuneus, cuneus, parietal and occipital cortices and in hypermetabolic regions in putamen, cerebellar vermis and cortex and pons (Fig. 3b). DLBRP was additionally comprised of hypometabolic regions in inferior temporal cortices and hypermetabolic regions in hippocampi, parahippocampi, insula and amygdala. The overlap between DLBRP and PDCP was seen in the hypometabolic region of the precuneus and hypermetabolic region of the cerebellal vermis and cortex.

3.3. ADRP contribution to DLBRP expression

ADRP expression differed in validation groups ($F(2, 108) = 10.3$, $p <$

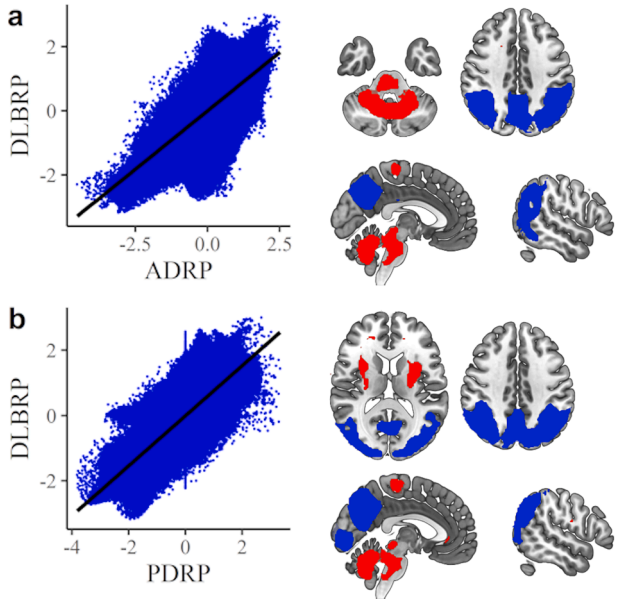

Fig. 3. Comparison between dementia with Lewy bodies related pattern (DLBRP) and other metabolic patterns. (A) Voxel-wise correlation and topographic overlap between DLBRP and Alzheimer's disease-related pattern (ADRP). (B) Voxel-wise correlation and topographic overlap between DLBRP and PDRP. The areas with overlapping hypometabolic activity are color-coded blue and the areas with overlapping hypermetabolic activity are color-coded red. (For interpretation of the references to color in this figure legend, the reader is referred to the web version of this article.)

0.001) even after controlling for age, sex and MMSE differences between groups and post hoc comparisons showed that covariate adjusted mean ADRP expression was significantly higher in both DLB2 (difference = 2.6, $t = 4.5$, $p < 0.001$) and AD (difference = 2.1, $t = 3.4$, $p = 0.002$) compared to NC2, but not between DLB2 and AD (difference = 0.6, $t = 1.7$, $p = 0.18$) (Fig. S1).

DLBRP ⊥ ADRP was defined as a linear combination of PC1 (22.5% VAF, $\beta = 0.94$) and PC3 (6.8% VAF, $\beta = 0.34$) and was characterized by relatively reduced metabolic activity in the occipital and left superior temporal cortex which co-varied with relatively increased metabolic activity in the bilateral inferior temporal cortices, hippocampi, parahippocampi, middle and anterior cingulate cortex (Fig. 4). This pattern's expression was significantly higher in DLB1 ($M = 5.0$, $SD = 2.0$) than NC1 ($M = 0.0$, $SD = 1.0$), $t(38) = 9.83$, $p < 0.001$ (Fig. 5). DLBRP ⊥ ADRP expression did not correlate with age ($r(18) = 0.00$, $p = 0.99$) nor MMSE ($r(13) = -0.13$, $p = 0.65$) in the DLB1.

DLBRP ⊥ ADRP expression differed in validation groups ($F(2, 108) = 46.5$, $p < 0.001$) even after controlling for age, sex and MMSE differences. Post hoc comparisons showed that covariate adjusted mean DLBRP ⊥ ADRP expression was significantly higher in DLB2 than in NC2 (difference = 2.3, $t = 4.18$, $p < 0.001$) and AD (difference = 3.0, $t = 9.44$, $p < 0.001$). There was no significant difference between AD and NC2 (difference = −0.64, $t = -1.12$, $p = 0.49$) (Fig. 5). DLBRP ⊥ ADRP expression did not correlate with age ($r(57) = 0.03$, $p = 0.84$) nor MMSE ($r(37) = -0.21$, $p = 0.20$) in the DLB2.

DLBRP and DLBRP ⊥ ADRP accurately differentiated between DLB2 and NC2 (AUC of 0.99 and 0.93, respectively). DLBRP moderately discriminated between DLB2 and AD (AUC = 0.72). DLBRP ⊥ ADRP accurately discriminated between DLB2 and AD (AUC = 0.87). Other performance metrics are given in Table 2.

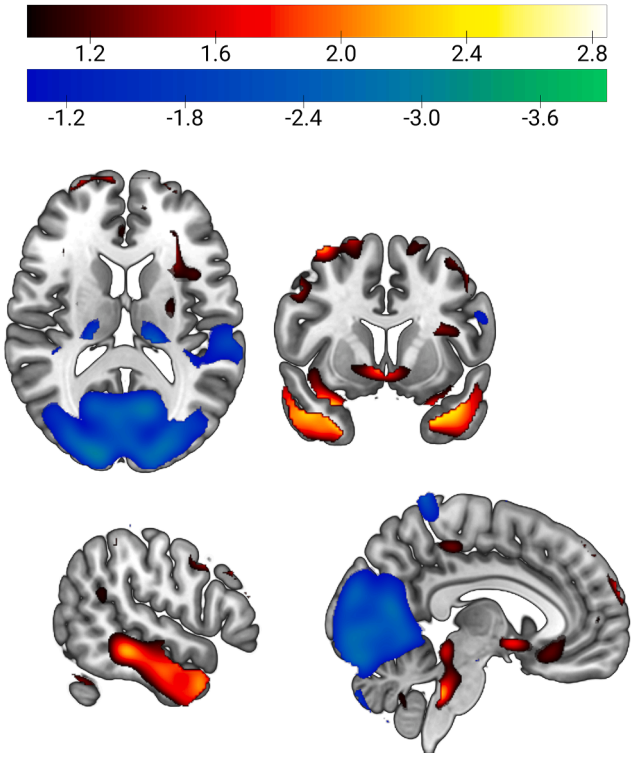

Fig. 4. Dementia with Lewy bodies-related pattern orthogonal to Alzheimer's disease-related pattern (DLBRP ⊥ ADRP). DLBRP ⊥ ADRP was characterized by relatively reduced metabolic activity (color-coded blue to green) in occipital and left superior temporal cortex which co-varied with relatively increased metabolic activity (color-coded red to white) in bilateral pallidum, right putamen, bilateral inferior temporal cortices, hippocampi, parahippocampi, middle and anterior cingulate cortex. (For interpretation of the references to color in this figure legend, the reader is referred to the web version of this article.)

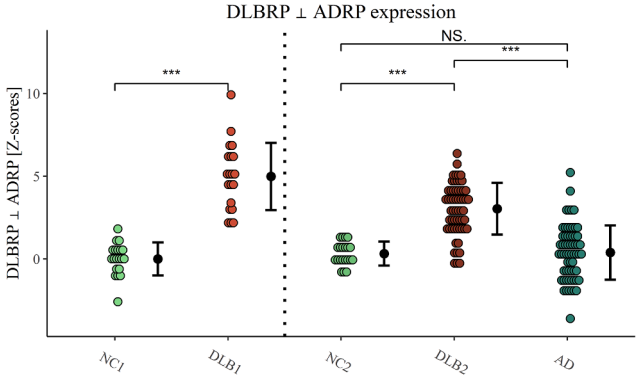

Fig. 5. Dementia with Lewy bodies-related pattern orthogonal to Alzheimer's disease-related pattern (DLBRP ⊥ ADRP) expression in identification (NC1 and DLB1) and validation (NC2, DLB2 and AD) groups. Data are Z-transformed based on the pattern expression in NC1 group. Means (SD) are presented to the right of individual data. NC – normal controls, DLB – dementia with Lewy bodies, AD – dementia due to Alzheimer's disease. ***p < 0.001, NS. – non-significant difference after adjusting for age, sex and MMSE.

3.4. The effect of Alzheimer's CSF profile in DLB patients on patterns expressions

A subset of 23 DLB patients from the validation group underwent CSF analysis and were classified as DLB with concomitant Alzheimer's

Table 2
Performance metrics of dementia with Lewy bodies-related pattern (DLBRP) and DLBRP orthogonal to Alzheimer's disease-related pattern (DLBRP ⊥ ADRP) expression.

	Pattern	AUC	Threshold	Spec.	Sens.	NPV	PPV
DLB2 vs NC2	DLBRP	0.99	1.42	100%	93%	84%	100%
DLB2 vs NC2	DLBRP ⊥ ADRP	0.93	1.58	100%	86%	72%	100%
DLB2 vs AD	DLBRP	0.72	3.90	73%	68%	71%	70%
DLB2 vs AD	DLBRP ⊥ ADRP	0.87	1.95	86%	80%	82%	84%

AUC – area under the curve, Threshold – optimal threshold according to Youden Index, Spec. – specificity, Sens. – sensitivity, NPV – negative predictive value, PPV – positive predictive value, DLB – dementia with Lewy bodies, NC – normal controls, AD – dementia due to Alzheimer's disease, DLBRP – DLB-related pattern, ADRP – AD-related pattern.

pathology (DLB-Alz), $n = 5$ (3 patients were A+/T+ and 2 were A+/T−), or DLB without concomitant Alzheimer's pathology (DLB-nonAlz), $n = 18$ (Table 3). The time between CSF and FDG PET imaging was 1 ± 3 months and it did not differ between the two groups ($t(17.1) = -1.48$, $p = 0.16$). The two groups did not differ in average age ($t(6.3) = 0.92$, $p = 0.39$), sex distribution ($p = 1.0$) or disease duration ($t(11) = 1.25$, $p = 0.23$). DLB-Alz had significantly higher expression of both DLBRP ($M = 6.1$, $SD = 0.9$ vs. $M = 4.5$, $SD = 1.7$, $t(13.8) = 2.88$, $p = 0.01$) and ADRP ($M = 6.9$, $SD = 1.1$ vs. $M = 5.1$, $SD = 1.7$, $t(10) = 2.87$, $p = 0.02$) compared to DLB-nonAlz. There was no statistically significant difference in expression of DLBRP ⊥ ADRP ($M = 3.9$, $SD = 1.1$ vs. $M = 3.0$, $SD = 1.7$, $t(7.3) = 1.27$, $p = 0.14$) (Fig. 6). Exploratory SPM analysis ($p \leq 0.01$ (unc.)) revealed clusters of decreased metabolic activity in DLB-Alz in bilateral middle and superior temporal gyri, and clusters of increased metabolic activity in right frontal middle orbital cortex and cerebellar cortex (Fig. S2).

3.5. Correlation between DLB metabolic patterns and survival time

During the available follow-up time, 32 patients out of 59 in the validation dataset died. The median survival from imaging was 657 days (range: 19–2297 days) and 1223 days (range: 29–2622 days) from first exam. We did not observe any correlation between the survival time and age ($r(30) = -0.19$, $p = 0.61$), disease duration ($r(27) = -0.03$, $p = 0.86$), MMSE ($r(21) = -0.10$, $p = 0.78$), or sex ($H(1) = 0.34$, $p = 0.78$). However, there was a significant moderate correlation between DLBRP ($r(30) = -0.43$, $p = 0.04$) and DLBRP ⊥ ADRP ($r(30) = -0.44$, $p = 0.04$) and survival time (Fig. 7). Reported p values are corrected for false discovery rate.

Table 3
Demographic data of subset of DLB participants with CSF analysis.

	DLB-Alz	DLB-nonAlz
N	5	18
Age (y)	76.6 ± 5.9	73.9 ± 5.7
Sex (f/m)	1/4	6/12
Disease duration (y)	4.8 ± 1.3	3.8 ± 2.1 (n = 17)
$A\beta_{42}$ (pg/ml)	532 ± 59	1038 ± 246
p-Tau (pg/ml)	50 ± 32	48 ± 21
t-Tau (pg/ml)	357 ± 218	320 ± 174
A+/T+	3/5	0/18
A+/T−	2/5	0/18

All the data is presented as mean ± SD. DLB-Alz – dementia with Lewy bodies with concomitant Alzheimer's pathology, DLB-nonAlz – DLB without concomitant Alzheimer's pathology, CSF – cerebrospinal fluid, $A\beta_{42}$ – amyloid β_{42}, p-Tau – phosphorylated tau, t-Tau – total tau, A – amyloid, T – tau.

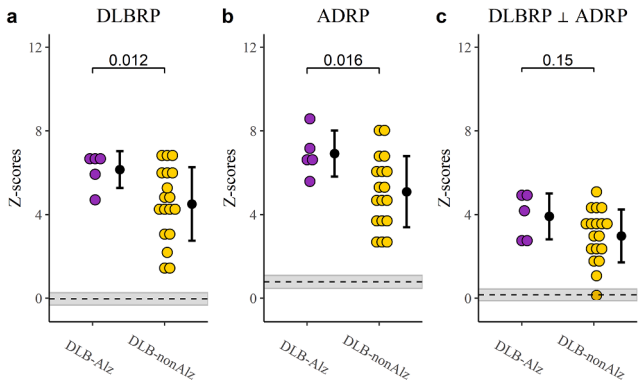

Fig. 6. Pattern expression in dementia with Lewy bodies (DLB) patients with and without concomitant Alzheimer's pathology. (a) Dementia with Lewy bodies-related pattern (DLBRP), (b) Alzheimer's disease-related pattern (ADRP) and (c) DLBRP orthogonal to ADRP (DLBRP ⊥ ADRP) expression. Differences between groups are given as p values. Data are Z-transformed based on the pattern expression in NC1 group. Means (SD) are presented to the right of individual data. Means of combined NC groups are presented as dashed lines and 95% confidence intervals as shaded areas. DLB-Alz – DLB with concomitant Alzheimer's pathology, DLB-nonAlz – DLB without concomitant Alzheimer's pathology.

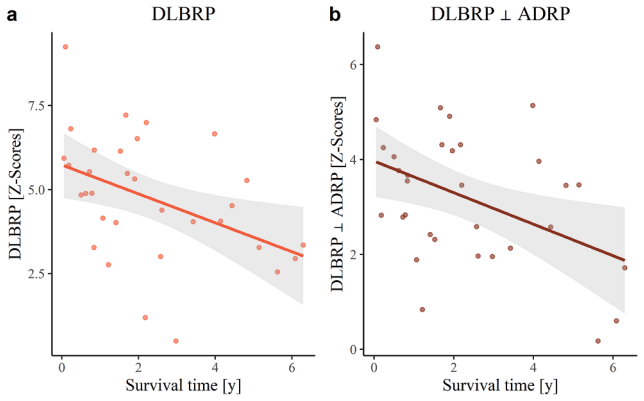

Fig. 7. Correlation analysis between pattern expression and survival time. (a) Correlation between dementia with Lewy bodies-related pattern (DLBRP) expression and survival time. (b) Correlation between DLBRP orthogonal to Alzheimer's disease-related pattern (DLBRP ⊥ ADRP) expression and survival time. Each dot represents an individual patient's data and the lines and shaded areas correspond to the fit of a linear regression with 95% confidence interval.

4. Discussion

In this study we identified and validated a metabolic biomarker of DLB in a large cohort of DLB patients. We explored its topographic relationship to metabolic brain patterns characteristic for syndromes with similar/overlapping clinical presentations, i. e. ADRP, PDRP and PDCP. We also examined an influence of concomitant Alzheimer's pathology on the pattern expression scores and lastly we studied prognostic value of DLBRP expression.

The DLBRP was characterized by relatively reduced bilateral metabolic activity in the occipital, inferior parietal and inferior temporal cortices and precuneus. This co-varied with relatively increased metabolic activity in the bilateral pallidum, putamen, amygdala, hippocampi, parahippocampi, cerebellar vermis and cortex and pons. Although the topography is similar to a DLB pattern described by Iizuka et Kameyama (Iizuka and Kameyama, 2020), our DLBRP showed additional hypometabolism in the inferior temporal lobes and

hypermetabolism in the cerebellum. Patients in our cohort had lower MMSE scores than those in Iizuka's cohort. This can account for more pronounced metabolic changes in our pattern. Topography of our DLBRP is similar to findings from Kang et al., who included similarly cognitively impaired DLB patients and used a modified SSM/PCA procedure (Kang et al., 2021). Cerebellar hypermetabolism was previously observed in DLB patients (Miyazawa et al., 2010; Ye et al., 2020) and spatial covariance pattern of brain perfusion that correlates with cognitive decline in DLB includes relative increases in the cerebellum (Taylor et al., 2013). Similarly, it has been shown that increased cerebellar activity is a compensatory mechanism to cognitive impairment in AD (Jacobs et al., 2018). The role of the cerebellum and the contribution of different regions to cognitive impairment in DLB, however, remains to be fully elucidated in future studies.

We studied the relationship of the newly identified DLBRP to three patterns characterized in clinically overlapping syndromes: ADRP, PDRP and PDCP. We observed a significant correlation between DLBRP and ADRP on a voxel-by-voxel basis, which was not unexpected since it is known that the hypometabolic profile is similar, but not the same, between the two diseases (Nestor et al., 2018). We also observed a correlation with PDRP, which was not surprising since all of our patients exhibited signs of parkinsonism and PDRP reflects the severity of parkinsonism (Schindlbeck and Eidelberg, 2018). Interestingly, DLBRP did not correlate with the cognitive pattern observed in PD − PDCP nor was there any correlation between PDCP expression and MMSE scores in DLB patients ($r = -0.23$, $p = 0.17$). Additionally, we noted that the results of DLBRP vs. PDRP/PDCP in our study are not impacted by differences in mean disease duration.

Another resting state network, which loss is commonly involved in cognitive impairment is the default mode network (DMN) (Carli et al., 2021). DMN is, however, intact in DLB, as suggested by a recent *meta*-analysis (Ma et al., 2022). On the other hand, PDCP shares topographical similarities with ventral part of the DMN with additional changes in lateral prefrontal, posterior parietal and medial temporal regions and both components are important for cognitive impairment in PD (Schindlbeck et al., 2021). Histopathologically, both PDD and DLB are characterized by Lewy body pathology, but with more severe limbic and neocortical involvement in the latter (Fan et al., 2021). Furthermore, different α-synuclein strains were reported in PDD and DLB (Van der Perren et al., 2020). Concomitant Alzheimer's pathology is also more common in DLB (Fan et al., 2021). Lastly, while neuropsychological profile can be similar in the two syndromes (Fields, 2017), a *meta*-analysis suggested, that on a group level there is a more severe impairment in executive functions in PDD and in memory and language in DLB (Brønnick, 2015). Our findings support the notion of a different underlying mechanism of cognitive dysfunction in DLB in comparison to PD. However, these observations should be further addressed in future research, preferably with a direct comparison of metabolic changes in PDD and DLB patients. Multiple linear regression analysis further confirmed that ADRP and PDRP both significantly contributed to DLBRP voxel weights, accounting for 24% and 37% variance, respectively. This leaves a remainder of approximately 35% of the variance unexplained, which might represent DLB-specific changes.

We observed that ADRP expression was elevated in DLB patients, probably on the account of overlapping pathology, topography of neurodegeneration and clinical presentation. Elevated ADRP expression in DLB patients in comparison to NC has been reported before (Katako et al., 2018; Lau et al., 2021). To account for overlapping topography we used an orthogonalization procedure to remove the contribution of AD-network and re-derived a pattern reflecting the "pure" DLB pathology, i.e. DLBRP ⊥ ADRP. This pattern was characterized by relatively reduced metabolic activity in the occipital and superior temporal cortices which co-varied with relatively increased metabolic activity in the bilateral pallidum, right putamen, bilateral inferior temporal cortices, parahippocampal area and middle and anterior cingulate cortex. Occipital cortex was the most prominent region included in DLBRP ⊥ ADRP, which is in line with previous studies that have shown that occipital hypoperfusion and hypometabolism is a distinct DLB feature (Arnaoutoglou et al., 2019). It was shown before that occipital perfusion and metabolism does not differ between amyloid negative and amyloid positive DLB patients (Donaghy et al., 2018), or between different neuropathological Lewy body disease subtypes (Graff-Radford et al., 2020). The effect of Alzheimer's pathology on DLBRP was further explored in a small group of DLB patients with Alzheimer's CSF changes. This group of patients exhibited higher expression of both ADRP and DLBRP in comparison to patients without concomitant Alzheimer's pathology. However, the two groups did not differ in the expression of DLBRP ⊥ ADRP, which presumably reflects the DLB-specific metabolic changes.

DLBRP expression was elevated in DLB patients in identification and validation cohorts, but not in NC or AD after accounting for differences in age, sex, and cognitive impairment. Based solely on the DLBRP expression we could very accurately discriminate between DLB and NC, comparable to other 2-[^{18}F]FDG PET studies (Etminani et al., 2022; Iizuka and Kameyama, 2020). The discriminatory power of DLBRP against NC was reduced after accounting for ADRP overlap, suggesting that the whole DLBRP is needed for an accurate separation of DLB and NC. On the contrary, the diagnostic accuracy of DLB versus AD greatly improved after removing ADRP, showing DLBRP ⊥ ADRP value in differential diagnosis. The sensitivity (80%) and specificity (86%) of DLBRP ⊥ ADRP to distinguish DLB from AD is comparable to DaTSCAN™ with sensitivity of 78% and specificity of 90% (McKeith et al., 2017). 2-[^{18}F]FDG PET also provides additional diagnostic value in discrimination between DLB and other parkinsonian syndromes (Caminiti et al., 2017). Furthermore, in contrast to DaTSCAN™ (Ziebell et al., 2013), 2-[^{18}F]FDG PET disease specific pattern expression scores, correlate well with the measures of clinical impairment.

In current clinical practice 2-[^{18}F]FDG PET scans are still mostly assessed visually with the help of semi-quantitative methods, which improve diagnostic accuracy (Perani et al., 2014), but still an expert reader is mandatory. On the other hand, methods that enable quantification on an individual level, such as SSM/PCA, provide the reader with an exact score to aid the diagnosis, and to be used for following disease progression or even treatment response (e.g. Ge et al., 2020; Matthews et al., 2021). Several other methods for automated assessment and computer-aided diagnosis, such as volumetric region of interest (VROI)-based analysis and calculation of Bayesian factor (Massa et al., 2022) or deep learning (Etminani et al., 2022) have been proposed. A head-to-head comparison between different methods and validation in independent datasets would be desirable before successful integration to routine clinical work-up.

Furthermore, DLBRP expression negatively correlated with MMSE in both the identification and validation cohorts with similar correlation coefficients (although we lacked statistical power in the former cohort). After removing the AD component this correlation was lost, suggesting a detrimental effect of Alzheimer's related neurodegeneration in regions involved in both patterns on cognitive impairment in DLB. Since DLB is related to a less favourable prognosis than AD and prognostic biomarkers for DLB are lacking (Mueller et al., 2017), we also aimed to explore the prognostic value of DLB patterns, which has not been done before. We found a significant correlation between DLBRP expression and survival time. A similar correlation coefficient was observed for DLBRP ⊥ ADRP expression, implicating that DLB-specific metabolic changes are driving the overall survival in DLB. The prognostic value of DLBRP and DLBRP ⊥ ADRP needs to be further examined in prospective settings, by including patients in earlier phases of the disease.

This study is not without limitations. Because this was a retrospective study and we did not have data on *post mortem* brain examination, we had to rely on the clinical records when making a diagnosis of DLB. The accuracy of the diagnosis was improved with a long-term follow-up by a dementia specialist. Furthermore, all of our patients with DLB exhibited signs of parkinsonism, which does eventually occur in over 85% of

patients (McKeith et al., 2017), but not all. Thus, our cohort does not represent the entire DLB spectrum. Additionally, the mean interval between CSF analysis and 2-[^{18}F]FDG PET imaging was 8 months. However, previous studies have shown a longitudinal stability of Alzheimer's CSF biomarkers up to 4 years from baseline (Lleó et al., 2019; Mattsson et al., 2012). The group of DLB patients with available information on CSF biomarkers was small. The presented results on the effect of Alzheimer's pathology on pattern expression are thus exploratory and should be validated in larger sample. All patients were recruited from a single institution. Therefore, the value of DLBRP and DLBRP ⊥ ADRP as metabolic biomarkers should be further studied and validated in other populations.

5. Conclusions

In this study we derived a metabolic brain biomarker characteristic for DLB, which expression can be prospectively quantified and used to accurately differentiate between DLB and NC. More importantly, it can differentiate between DLB and AD when appropriately accounting for network similarities between the two diseases. We have shown that DLBRP shares some similarities with both ADRP and PDRP, but is also characterized by DLB-specific changes that are not a part of either aforementioned patterns. We have also shown that the expression of DLBRP correlates with cognitive impairment. This correlation disappears with the removal of AD contribution to the pattern, suggesting a similar underlying mechanism involved with cognitive dysfunction in both diseases. Conversely, both DLB patterns (with and without AD contribution) correlated with survival time; this demonstrates the prognostic value of this biomarker and suggests a more detrimental contribution of DLB-specific changes to the patients' survival.

CRediT authorship contribution statement

Matej Perovnik: Conceptualization, Software, Formal analysis, Data curation, Writing – original draft, Writing – review & editing, Visualization. **Petra Tomše:** Resources, Data curation, Writing – review & editing. **Jan Jamšek:** Resources, Writing – review & editing. **Chris Tang:** Methodology, Writing – review & editing. **David Eidelberg:** Methodology, Writing – review & editing, Supervision. **Maja Trošt:** Conceptualization, Writing – review & editing, Supervision, Funding acquisition.

Declaration of Competing Interest

The authors declare that they have no known competing financial interests or personal relationships that could have appeared to influence the work reported in this paper.

Acknowledgements

We wish to thank Assist. Prof. Milica G. Kramberger, MD, PhD and other members of the Center for Cognitive impairment for patients' referrals. The authors wish to thank: Luka Jensterle, BSc for his help with preparation of 2-[^{18}F]FDG PET scans; Boštjan Simonič, BSc Ivan Slodnjak, BSc and Sebastijan Rep, PhD for their help in the acquisition of PET and SPECT images; Andreja Emeršič, MPharm for CSF analysis; as well as the clinicians and nurses from the Department for Neurology and Department for Nuclear Medicine, University Medical Center Ljubljana who made our research possible. The authors also thank Alice Oh, BA for her valuable editorial assistance in preparing the manuscript.

Funding

This work was supported by The Slovenian Research Agency (ARRS) through grants P1-0389, J7-2600 and J7-3150.

Availability of data and material

The datasets generated and analysed during the current study are available from the corresponding author on reasonable request and signing a data-sharing agreement.

Ethics approval and consent to participate

The study was approved by Slovenian National Ethics Committee (0120-584/2019/5). All patients gave informed consent.

Conflicts of interest

Trošt M has received grants from the Slovenian Research Agency. The payment was made to University Medical Center Ljubljana. Trošt M has received consulting fees from STADA, AbbVie, and Guidepoint, all related to advanced Parkinson's disease treatment. The payment was made directly to Trošt M. Trošt M has received honoraria for lectures from STADA, AbbVie and Britannia Pharmaceuticals Ltd, all related to advanced Parkinson's disease treatment. The payment was made directly to Trošt M. Trošt M has received financial support for attending meetings and/or travel from AbbVie and Medtronic. The payment was made to University Medical Center Ljubljana. Trošt M is a member of the Advisory Board for AbbVie. The payment was made directly to Trošt M. All funding received by Trošt M is unrelated to the manuscript. Eidelberg D has received grants from NIH (NINDS, NIADS). Eidelberg D receives consulting fees from MeiraGTx. Eidelberg D serves on the scientific advisory boards of and has received fees from The Michael J. Fox Foundation for Parkinson's Research and Ovid Therapeutics. All funding received by Eidelberg D is unrelated to the manuscript. Perovnik M, Tomše P, Jamšek J and Tang CC have no conflicts of interest to declare.

Appendix A. Supplementary data

Supplementary data to this article can be found online at https://doi.org/10.1016/j.nicl.2022.103080.

References

Arnaoutoglou, N.A., O'Brien, J.T., Underwood, B.R., 2019. Dementia with Lewy bodies — from scientific knowledge to clinical insights. Nat. Rev. Neurol. 15, 103–112. https://doi.org/10.1038/s41582-018-0107-7.

Brønnick, K., 2015. Cognitive profile in Parkinson's disease dementia. In: Emre, M. (Ed.), Cognitive Impairment and Dementia in Parkinson's Disease. Oxford University Press, pp. 27–45.

Brown, R.K.J., Bohnen, N.I., Wong, K.K., Minoshima, S., Frey, K.A., 2014. Brain PET in Suspected Dementia: Patterns of Altered FDG Metabolism. RadioGraphics 34, 684–701. https://doi.org/10.1148/rg.343135065.

Caminiti, S.P., Alongi, P., Majno, L., Volontè, M.A., Cerami, C., Gianolli, L., Comi, G., Perani, D., 2017. Evaluation of an optimized [18F]fluoro-deoxy-glucose positron emission tomography voxel-wise method to early support differential diagnosis in atypical Parkinsonian disorders. Eur. J. Neurol. 24, 1–8. https://doi.org/10.1111/ene.13269.

Carli, G., Tondo, G., Boccalini, C., Perani, D., 2021. Brain Molecular Connectivity in Neurodegenerative Conditions. Brain Sci. 11, 433. https://doi.org/10.3390/brainsci11040433.

Darcourt, J., Booij, J., Tatsch, K., Varrone, A., Vander Borght, T., Kapucu, Ö.L., Någren, K., Nobili, F., Walker, Z., Van Laere, K., 2010. EANM procedure guidelines for brain neurotransmission SPECT using 123I-labelled dopamine transporter ligands, version 2. Eur. J. Nucl. Med. Mol. Imaging 37, 443–450. https://doi.org/10.1007/s00259-009-1267-x.

Delacre, M., Lakens, D., Leys, C., 2017. Why Psychologists Should by Default Use Welch's t-test Instead of Student's t-test. Int. Rev. Soc. Psychol. 30, 92. https://doi.org/10.5334/irsp.82.

Donaghy, P.C., Firbank, M.J., Thomas, A.J., Lloyd, J., Petrides, G., Barnett, N., Olsen, K., O'Brien, J.T., 2018. Clinical and imaging correlates of amyloid deposition in dementia with Lewy bodies. Mov. Disord. 33, 1130–1138. https://doi.org/10.1002/mds.27403.

Etminani, Kobra, Soliman, Amira, Davidsson, Anette, Chang, Jose R., Martínez-Sanchis, Begoña, Byttner, Stefan, Camacho, Valle, Bauckneht, Matteo, Stegeran, Roxana, Ressner, Marcus, Agudelo-Cifuentes, Marc, Chincarini, Andrea, Brendel, Matthias, Rominger, Axel, Bruffaerts, Rose, Vandenberghe, Rik, Kramberger, Milica G., Trost, Maja, Nicastro, Nicolas, Frisoni, Giovanni B., Lemstra, Afina W., van Berckel, Bart N.M., Pilotto, Andrea, Padovani, Alessandro,

Morbelli, Silvia, Aarsland, Dag, Nobili, Flavio, Garibotto, Valentina, Ochoa-Figueroa, Miguel, 2022. A 3D deep learning model to predict the diagnosis of dementia with Lewy bodies, Alzheimer's disease, and mild cognitive impairment using brain 18F-FDG PET. Eur. J. Nucl. Med. Mol. Imaging. 49 (2), 563–584.
Fan, T.-S., Liu, S.C.-H., Wu, R.-M., 2021. Alpha-Synuclein and Cognitive Decline in Parkinson Disease. Life 11, 1239. https://doi.org/10.3390/life11111239.
Fields, J.A., 2017. Cognitive and Neuropsychiatric Features in Parkinson's and Lewy Body Dementias. Arch. Clin. Neuropsychol. 32, 786–801. https://doi.org/10.1093/arclin/acx085.
Ge, J., Wang, M., Lin, W., Wu, P., Guan, Y., Zhang, H., Huang, Z., Yang, L., Zuo, C., Jiang, J., Rominger, A., Shi, K., 2020. Metabolic network as an objective biomarker in monitoring deep brain stimulation for Parkinson's disease: a longitudinal study. EJNMMI Res. 10, 131. https://doi.org/10.1186/s13550-020-00722-1.
Graff-Radford, J., Lesnick, T.G., Savica, R., Chen, Q., Ferman, T.J., Przybelski, S.A., Jones, D.T., Senjem, M.L., Gunter, J.L., Kremers, W.K., Jack, C.R., Lowe, V.J., Petersen, R.C., Knopman, D.S., Boeve, B.F., Murray, M.E., Dickson, D.W., Kantarci, K., 2020. 18F-fluorodeoxyglucose positron emission tomography in dementia with Lewy bodies. Brain Commun. 2, 1–8. https://doi.org/10.1093/braincomms/fcaa040.
Grömping, U., 2006. Relative Importance for Linear Regression in R : The Package relaimpo. J. Stat. Softw. 17, 1–27. https://doi.org/10.18637/jss.v017.i01.
Hansson, O., 2021. Biomarkers for neurodegenerative diseases. Nat. Med. 27, 954–963. https://doi.org/10.1038/s41591-021-01382-x.
Hepp, Dagmar H., Vergoossen, Dana L.E., Huisman, Evelien, Lemstra, Afina W., Berendse, Henk W., Rozemuller, Annemieke J., Foncke, Elisabeth M.J., van de Berg, Wilma D.J., 2016. Distribution and Load of Amyloid-β Pathology in Parkinson Disease and Dementia with Lewy Bodies. J. Neuropathol. Exp. Neurol. 75 (10), 936–945.
Huang, C., Mattis, P., Tang, C., Perrine, K., Carbon, M., Eidelberg, D., 2007. Metabolic brain networks associated with cognitive function in Parkinson's disease. Neuroimage 34, 714–723. https://doi.org/10.1016/j.neuroimage.2006.09.003.
Iizuka, Tomomichi, Kameyama, Masashi, 2020. Spatial metabolic profiles to discriminate dementia with Lewy bodies from Alzheimer disease. J. Neurol. 267 (7), 1960–1969.
Jack, Clifford R., Bennett, David A., Blennow, Kaj, Carrillo, Maria C., Dunn, Billy, Haeberlein, Samantha Budd, Holtzman, David M., Jagust, William, Jessen, Frank, Karlawish, Jason, Liu, Enchi, Molinuevo, Jose Luis, Montine, Thomas, Phelps, Creighton, Rankin, Katherine P., Rowe, Christopher C., Scheltens, Philip, Siemers, Eric, Snyder, Heather M., Sperling, Reisa, Elliott, Cerise, Masliah, Eliezer, Ryan, Laurie, Silverberg, Nina, 2018. NIA-AA Research Framework: Toward a biological definition of Alzheimer's disease. Alzheimer's Dement. 14 (4), 535–562.
Jacobs, H.I.L., Hopkins, D.A., Mayrhofer, H.C., Bruner, E., van Leeuwen, F.W., Raaijmakers, W., Schmahmann, J.D., 2018. The cerebellum in Alzheimer's disease: evaluating its role in cognitive decline. Brain 141, 37–47. https://doi.org/10.1093/brain/awx194.
Jellinger, Kurt A., 2018. Dementia with Lewy bodies and Parkinson's disease-dementia: current concepts and controversies. J. Neural Transmission Springer Vienna 125 (4), 615–650.
Kang, S.W., Jeon, S., Lee, Y., Park, M., Baik, K., Jung, J.H., Chung, S.J., Yoo, H.S., Jeong, S.H., Yun, M., Lee, P.H., Sohn, Y.H., Evans, A.C., Ye, B.S., 2021. Implication of metabolic and dopamine transporter PET in dementia with Lewy bodies. Sci. Rep. 11, 14394. https://doi.org/10.1038/s41598-021-93442-y.
Katako, A., Shelton, P., Goertzen, A.L., Levin, D., Bybel, B., Aljuaid, M., Yoon, H.J., Kang, D.Y., Kim, S.M., Lee, C.S., Ko, J.H., 2018. Machine learning identified an Alzheimer's disease-related FDG-PET pattern which is also expressed in Lewy body dementia and Parkinson's disease dementia. Sci. Rep. 8, 1–13. https://doi.org/10.1038/s41598-018-31653-6.
Ko, Ji Hyun, Spetsieris, Phoebe, Ma, Yilong, Dhawan, Vijay, Eidelberg, David, Chen, Robert, 2014. Quantifying significance of topographical similarities of disease-related brain metabolic patterns. PLoS One 9 (1), e88119.
Lau, A., Beheshti, I., Modirrousta, M., Kolesar, T.A., Goertzen, A.L., Ko, J.H., 2021. Alzheimer's Disease-Related Metabolic Pattern in Diverse Forms of Neurodegenerative Diseases. Diagnostics 11, 2023. https://doi.org/10.3390/diagnostics11112023.
Lee, Y., Jeon, S., Yoo, H.S., Chung, S.J., Lee, S.-K., Lee, P.H., Sohn, Y.H., Yun, M., Evans, A.C., Ye, B.S., 2018. Amyloid-β-related and unrelated cortical thinning in dementia with Lewy bodies. Neurobiol. Aging 72, 32–39. https://doi.org/10.1016/j.neurobiolaging.2018.08.007.
Lemstra, A.W., de Beer, M.H., Teunissen, C.E., Schreuder, C., Scheltens, P., van der Flier, W.M., Sikkes, S.A.M., 2017. Concomitant AD pathology affects clinical manifestation and survival in dementia with Lewy bodies. J. Neurol. Neurosurg. Psychiatry 88, 113–118. https://doi.org/10.1136/jnnp-2016-313775.
Lleó, A., Alcolea, D., Martínez-Lage, P., Scheltens, P., Parnetti, L., Poirier, J., Simonsen, A.H., Verbeek, M.M., Rosa-Neto, P., Slot, R.E.R., Tainta, M., Izaguirre, A., Reijs, B.L.R., Farotti, L., Tsolaki, M., Vandenbergue, R., Freund-Levi, Y., Verhey, F.R. J., Clarimón, J., Fortea, J., Frolich, L., Santana, I., Molinuevo, J.L., Lehmann, S., Visser, P.J., Teunissen, C.E., Zetterberg, H., Blennow, K., 2019. Longitudinal cerebrospinal fluid biomarker trajectories along the Alzheimer's disease continuum in the BIOMARKAPD study. Alzheimer's Dement. 15, 742–753. https://doi.org/10.1016/j.jalz.2019.01.015.
Ma, W., Tian, M., Yao, Q., Li, Q., Tang, F., Xiao, C., Shi, J., Chen, J., 2022. Neuroimaging alterations in dementia with Lewy bodies and neuroimaging differences between dementia with Lewy bodies and Alzheimer's disease: An activation likelihood estimation meta-analysis. CNS Neurosci. Ther. 28, 183–205. https://doi.org/10.1111/cns.13775.
Massa, F., Chincarini, A., Bauckneht, M., Raffa, S., Peira, E., Arnaldi, D., Pardini, M., Pagani, M., Orso, B., Donegani, M.I., Brugnolo, A., Biassoni, E., Mattioli, P., Girtler, N., Guerra, U.P., Morbelli, S., Nobili, F., 2022. Added value of semiquantitative analysis of brain FDG-PET for the differentiation between MCI-Lewy bodies and MCI due to Alzheimer's disease. Eur. J. Nucl. Med. Mol. Imaging 49, 1263–1274. https://doi.org/10.1007/s00259-021-05568-w.
Matthews, D.C., Ritter, A., Thomas, R.G., Andrews, R.D., Lukic, A.S., Revta, C., Kinney, J. W., Tousi, B., Leverenz, J.B., Fillit, H., Zhong, K., Feldman, H.H., Cummings, J., 2021. Rasagiline effects on glucose metabolism, cognition, and tau in Alzheimer's dementia. Alzheimer's Dement. Transl. Res. Clin. Interv. 7, 1–12. https://doi.org/10.1002/trc2.12106.
Mattsson, N., Portelius, E., Rolstad, S., Gustavsson, M., Andreasson, U., Stridsberg, M., Wallin, A., Blennow, K., Zetterberg, H., 2012. Longitudinal Cerebrospinal Fluid Biomarkers over Four Years in Mild Cognitive Impairment. J. Alzheimer's Dis. 30, 767–778. https://doi.org/10.3233/JAD-2012-120019.
McKeith, I.G., Boeve, B.F., Dickson, D.W., Halliday, G., Taylor, J.-P., Weintraub, D., Aarsland, D., Galvin, J., Attems, J., Ballard, C.G., Bayston, A., Beach, T.G., Blanc, F., Bohnen, N., Bonanni, L., Bras, J., Brundin, P., Burn, D., Chen-Plotkin, A., Duda, J.E., El-Agnaf, O., Feldman, H., Ferman, T.J., Ffytche, D., Fujishiro, H., Galasko, D., Goldman, J.G., Gomperts, S.N., Graff-Radford, N.R., Honig, L.S., Iranzo, A., Kantarci, K., Kaufer, D., Kukull, W., Lee, V.M.Y., Leverenz, J.B., Lewis, S., Lippa, C., Lunde, A., Masellis, M., Masliah, E., McLean, P., Mollenhauer, B., Montine, T.J., Moreno, E., Mori, E., Murray, M., O'Brien, J.T., Orimo, S., Postuma, R.B., Ramaswamy, S., Ross, O.A., Salmon, D.P., Singleton, A., Taylor, A., Thomas, A., Tiraboschi, P., Toledo, J.B., Trojanowski, J.Q., Tsuang, D., Walker, Z., Yamada, M., Kosaka, K., 2017. Diagnosis and management of dementia with Lewy bodies Fourth consensus report of the DLB Consortium. Neurology 89, 88–100. https://doi.org/10.1212/WNL.0000000000004058.
Meles, S.K., Kok, J.G., Renken, R.J., Leenders, K.L., 2021. From Positron to Pattern: A Conceptual and Practical Overview of 18F-FDG PET Imaging and Spatial Covariance Analysis. In: Dierckx, R.A.J.O., Otte, A., de Vries, E.F.J., van Waarde, A., Leenders, K. L. (Eds.), PET and SPECT in Neurology. Springer International Publishing, Cham, pp. 73–104. https://doi.org/10.1007/978-3-030-53168-3_4.
Meles, S.K., Pagani, M., Arnaldi, D., De Carli, F., Dessi, B., Morbelli, S., Sambuceti, G., Jonsson, C., Leenders, K.L., Nobili, F., 2017. The Alzheimer's disease metabolic brain pattern in mild cognitive impairment. J. Cereb. Blood Flow Metab. 37, 3643–3648. https://doi.org/10.1177/0271678X17732508.
Miyazawa, N., Shinohara, T., Nagasaka, T., Hayashi, M., 2010. Hypermetabolism in Patients With Dementia With Lewy Bodies. Clin. Nucl. Med. 35, 490–493. https://doi.org/10.1097/RLU.0b013e3181e05dbc.
Morbelli, Silvia, Chincarini, Andrea, Brendel, Matthias, Rominger, Axel, Bruffaerts, Rose, Vandenberghe, Rik, Kramberger, Milica G., Trost, Maja, Garibotto, Valentina, Nicastro, Nicolas, Frisoni, Giovanni B., Lemstra, Afina W., Zande, Jessica, Pilotto, Andrea, Padovani, Alessandro, Garcia-Ptacek, Sara, Savitcheva, Irina, Ochoa-Figueroa, Miguel A., Davidsson, Annette, Camacho, Valle, Peira, Enrico, Arnaldi, Dario, Bauckneht, Matteo, Pardini, Matteo, Sambuceti, Gianmario, Aarsland, Dag, Nobili, Flavio, 2019. Metabolic patterns across core features in dementia with lewy bodies. Ann. Neurol. 85 (5), 715–725.
Mueller, C., Ballard, C., Corbett, A., Aarsland, D., 2017. The prognosis of dementia with Lewy bodies. Lancet Neurol. 16, 390–398. https://doi.org/10.1016/S1474-4422(17)30074-1.
Nestor, Peter J., Altomare, Daniele, Festari, Cristina, Drzezga, Alexander, Rivolta, Jasmine, Walker, Zuzana, Bouwman, Femke, Orini, Stefania, Law, Ian, Agosta, Federica, Arbizu, Javier, Boccardi, Marina, Nobili, Flavio, Frisoni, Giovanni Battista, 2018. Clinical utility of FDG-PET for the differential diagnosis among the main forms of dementia. Eur. J. Nucl. Med. Mol. Imaging 45 (9), 1509–1525.
Oppedal, Ketil, Borda, Miguel G, Ferreira, Daniel, Westman, Eric, Aarsland, Dag, 2019. European DLB consortium: diagnostic and prognostic biomarkers in dementia with Lewy bodies, a multicenter international initiative. Neurodegener. Dis. Manag. 9 (5), 247–250.
Perani, D., Della Rosa, P.A., Cerami, C., Gallivanone, F., Fallanca, F., Vanoli, E.G., Panzacchi, A., Nobili, F., Pappatà, S., Marcone, A., Garibotto, V., Castiglioni, I., Magnani, G., Cappa, S.F., Gianolli, L., Drzezga, A., Perneczky, R., Didic, M., Guedj, E., Van Berckel, B.N., Ossenkoppele, R., Morbelli, S., Frisoni, G., Caroli, A., 2014. Validation of an optimized SPM procedure for FDG-PET in dementia diagnosis in a clinical setting. NeuroImage. Clin. 6, 445–454. https://doi.org/10.1016/j.nicl.2014.10.009.
Perovnik, M., Rus, T., Tomše, P., Jensterle, L., Emeršič, A., Grmek, M., Jamšek, J., Kramberger, M.G., Pirtošek, Z., Trost, M., 2020. Identification and validation of Alzheimer's disease-related metabolic pattern in patients with pathologically confirmed Alzheimer's disease. Alzheimer's Dement. 16, 10–12. https://doi.org/10.1002/alz.042629.
R Core Team, 2019. R: A Language and Environment for Statistical Computing.
Raffa, S., Donegani, M.I., Borra, A., Miceli, A., Balma, M., Bauckneht, M., Morbelli, S., 2020. Role of [18F]-FDG PET in patients with atypical parkinsonism associated with dementia. Clin. Transl. Imaging 8, 107–122. https://doi.org/10.1007/s40336-020-00360-6.
Rakusa, M., Granda, G., Kogoj, A., Mlakar, J., Vodusek, D.B., 2006. Mini-Mental State Examination: standardization and validation for the elderly Slovenian population. Eur. J. Neurol. 13, 141–145. https://doi.org/10.1111/j.1468-1331.2006.01185.x.
Rizzo, G., Arcuti, S., Copetti, M., Alessandria, M., Savica, R., Fontana, A., Liguori, R., Logroscino, G., 2018. Accuracy of clinical diagnosis of dementia with Lewy bodies: a systematic review and meta-analysis. J. Neurol. Neurosurg. Psychiatry 89, 358–366. https://doi.org/10.1136/jnnp-2017-316844.
Robin, X., Turck, N., Hainard, A., Tiberti, N., Lisacek, F., Sanchez, J.-C., Müller, M., 2011. pROC: an open-source package for R and S+ to analyze and compare ROC curves. BMC Bioinformatics 12, 77. https://doi.org/10.1186/1471-2105-12-77.

Rorden, C., Brett, M., 2000. Stereotaxic Display of Brain Lesions. Behav. Neurol. 12, 191–200. https://doi.org/10.1155/2000/421719.
Schindlbeck, K.A., Eidelberg, D., 2018. Network imaging biomarkers: insights and clinical applications in Parkinson's disease. Lancet Neurol. 17, 629–640. https://doi.org/10.1016/S1474-4422(18)30169-8.
Schindlbeck, K.A., Vo, A., Mattis, P.J., Villringer, K., Marzinzik, F., Fiebach, J.B., Eidelberg, D., 2021. Cognition-Related Functional Topographies in Parkinson's Disease: Localized Loss of the Ventral Default Mode Network. Cereb. Cortex 31, 5139–5150. https://doi.org/10.1093/cercor/bhab148.
Shim, Y.S., Roe, C.M., Buckles, V.D., Morris, J.C., 2013. Clinicopathologic Study of Alzheimer's Disease: Alzheimer Mimics. J. Alzheimer's Dis. 35, 799–811. https://doi.org/10.3233/JAD-121594.
Spetsieris, P.G., Eidelberg, D., 2011. Scaled subprofile modeling of resting state imaging data in Parkinson's disease: Methodological issues. Neuroimage 54, 2899–2914. https://doi.org/10.1016/j.neuroimage.2010.10.025.
Taylor, J.-P., Colloby, S.J., McKeith, I.G., O'Brien, J.T., 2013. Covariant perfusion patterns provide clues to the origin of cognitive fluctuations and attentional dysfunction in Dementia with Lewy bodies. Int. Psychogeriatrics 25, 1917–1928. https://doi.org/10.1017/S1041610213001488.
Tomše, P., Jensterle, L., Grmek, M., Zaletel, K., Pirtošek, Z., Dhawan, V., Peng, S., Eidelberg, D., Ma, Y., Trošt, M., 2017. Abnormal metabolic brain network associated with Parkinson's disease: replication on a new European sample. Neuroradiology 59, 507–515. https://doi.org/10.1007/s00234-017-1821-3.
Trošt, M., Perovnik, M., Pirtošek, Z., 2019. Correlations of Neuropsychological and Metabolic Brain Changes in Parkinson's Disease and Other α-Synucleinopathies. Front. Neurol. 10, 1–10. https://doi.org/10.3389/fneur.2019.01204.
Van der Perren, Anke, Gelders, Géraldine, Fenyi, Alexis, Bousset, Luc, Brito, Filipa, Peelaerts, Wouter, Van den Haute, Chris, Gentleman, Steve, Melki, Ronald, Baekelandt, Veerle, 2020. The structural differences between patient-derived α-synuclein strains dictate characteristics of Parkinson's disease, multiple system atrophy and dementia with Lewy bodies. Acta Neuropathol 139 (6), 977–1000.
Vann Jones, S.A., O'Brien, J.T., 2014. The prevalence and incidence of dementia with Lewy bodies: a systematic review of population and clinical studies. Psychol. Med. 44, 673–683. https://doi.org/10.1017/S0033291713000494.
Varrone, A., Asenbaum, S., Vander Borght, T., Booij, J., Nobili, F., Någren, K., Darcourt, J., Kapucu, Ö.L., Tatsch, K., Bartenstein, P., Van Laere, K., 2009. EANM procedure guidelines for PET brain imaging using [18F]FDG, version 2. Eur. J. Nucl. Med. Mol. Imaging 36, 2103–2110. https://doi.org/10.1007/s00259-009-1264-0.
Watson, R., Colloby, S.J., 2016. Imaging in Dementia with Lewy Bodies: An Overview. J. Geriatr. Psychiatry Neurol. 29, 254–260. https://doi.org/10.1177/0891988716654984.
Wickham, H., 2016. ggplot2, Use R! Springer International Publishing, Cham. https://doi.org/10.1007/978-3-319-24277-4.
Ye, B.S., Lee, S., Yoo, H., Chung, S.J., Lee, Y.H., Choi, Y., Lee, P.H., Sohn, Y.H., Yun, M., 2020. Distinguishing between dementia with Lewy bodies and Alzheimer's disease using metabolic patterns. Neurobiol. Aging 87, 11–17. https://doi.org/10.1016/j.neurobiolaging.2019.10.020.
Ziebell, M., Andersen, B.B., Pinborg, L.H., Knudsen, G.M., Stokholm, J., Thomsen, G., Karlsborg, M., Høgh, P., Mørk, M.L., Hasselbalch, S.G., 2013. Striatal Dopamine Transporter Binding Does Not Correlate with Clinical Severity in Dementia with Lewy Bodies. J. Nucl. Med. 54, 1072–1076. https://doi.org/10.2967/jnumed.112.114025.
Zuber, V., Strimmer, K., 2011. High-Dimensional Regression and Variable Selection Using CAR Scores. Stat. Appl. Genet. Mol. Biol. 10, 1–25. https://doi.org/10.2202/1544-6115.1730.